Crystal symmetry of BiMnO₃: Electron diffraction study

Tadahiro Yokosawa,[1,*] Alexei A. Belik,[2] Toru Asaka,[1] Koji Kimoto,[1] Eiji Takayama-Muromachi,[2] and Yoshio Matsui[1]

[1]*High Voltage Electron Microscopy Station (HVEMS), National Institute for Materials Science (NIMS),*
1-1 Namiki, Tsukuba, Ibaraki 305-0044, Japan
[2]*Advanced Nano Materials Laboratory (ANML), National Institute for Materials Science (NIMS),*
1-1 Namiki, Tsukuba, Ibaraki 305-0044, Japan
(Received 28 March 2007; published 28 January 2008)

The crystal symmetry of $BiMnO_3$ was investigated by convergent-beam electron diffraction (CBED) and selected-area electron diffraction (SAED). CBED, which was used in order to discriminate the crystal axes of $BiMnO_3$ in this study, showed that $BiMnO_3$ belongs to point group $2/m$ with the c-glide plane perpendicular to the b axis, resulting in space group $C2/c$. In the SAED patterns, however, the very weak but sharp $h0l$ ($l=2n+1$) and broader $h0l$ ($h=2n+1$) reflections were observed, indicating the noncentrosymmetric long-range (space group $C2$) and short-range ordered structures ($P2$ or $P2_1$), respectively. This implies that the weak reflections had quite little influence on the CBED patterns. By substituting Sc for Mn, the long-range ordered structure persisted up to $BiMn_{0.6}Sc_{0.4}O_3$ at 300 K, but short-range ordered structure disappeared already in $BiMn_{0.9}Sc_{0.1}O_3$. In $BiMnO_3$ at 673 K, the long-range ordered structure persisted while the short-range ordered structure disappeared. Both $h0l$ ($l=2n+1$ and $h=2n+1$) reflections could not be detected in structurally related $BiScO_3$ and $BiCrO_3$ at 300 K indicating that they belong to centrosymmetric $C2/c$. This strongly suggests that the noncentrosymmetric long-range ordered structure ($C2$) of $BiMnO_3$ is attributed not only to Bi^{3+} ions with lone electron pair but also to Mn^{3+} ions, that is, to correlation between Bi^{3+} and Mn^{3+} ions. The results of this work are important for understanding multiferroic properties of $BiMnO_3$.

I. INTRODUCTION

Multiferroic materials have attracted tremendous interest because of their expected wide technological applications.[1] Two or all three of (anti)ferroelectricity, (anti)ferromagnetism, and ferroelasticity occur in multiferroic systems.[2] Perovskite $BiMnO_3$ is one of the most studied multiferroic compound.[3–23] $BiMnO_3$ is a well-established ferromagnet below $T_C \approx 100$ K.[3–5] The crystal structure of $BiMnO_3$ was determined from neutron powder diffraction data in noncentrosymmetric space group $C2$ [$a=9.53$ Å, $b=5.61$ Å, $c=9.85$ Å, and $\beta=110.67°$ at room temperature (RT)].[4,6] Space group $C2$ was assigned based on selected-area electron diffraction (SAED).[20] Note that effects of double diffraction were not taken into account during space group determination. In the mean time, it was reported by theoretical calculations that a multiferroic state can possibly occur in $BiMnO_3$ due to the existence of Bi^{3+} active electron pair (lone pair).[7] Ferroelectric hysteresis loop measurements reported in one paper gave polarization of 0.043 $\mu C/cm^2$ at 200 K, and $BiMnO_3$ was considered to be a ferroelectric material.[8] However, there is still no consensus on the ferroelectric Curie temperature (470 or 770 K).[9] Magnetoferroelectric feature of $BiMnO_3$ below T_C has also been investigated[5] as well as the phase transitions at 470 K (monoclinic to monoclinic without any symmetry change) and 770 K (monoclinic to orthorhombic).[5,10–12] However, despite the preparation of highly resistive $BiMnO_3$ thin films,[13] there are no other direct (hysteresis loop) confirmations of the ferroelectric properties of $BiMnO_3$.

The long-range orbital order in $BiMnO_3$ was proposed from the analysis of the crystal structure studied by neutron diffraction[4,6] and recently confirmed by resonant x-ray scattering studies on $BiMnO_3$ thin films where the resonant (003) peak persists up to 770 K.[9] Using SAED, high-resolution transmission electron microscopy (HRTEM), and electron energy-loss spectroscopy (EELS), it was revealed that polymorph phases found in $BiMnO_3$ (Ref. 10) can be achieved by knocking the oxygen atoms out of the $BiMnO_3$ sample by electron beam irradiation inside a transmission electron microscope (TEM).[14,15] The structural defects that may play important roles for ferroelectricity of the bulk $BiMnO_3$ sample were also investigated in terms of HRTEM and EELS.[16] Recently, it was pointed out that the centrosymmetric structure of $BiMnO_3$ can also be possible based on the structural analysis of structurally related $BiScO_3$ whose space group was determined to be $C2/c$ using neutron powder diffraction and SAED (Ref. 24) and based on the first-principles calculations.[21]

Regarding background to determination of the space group of $BiMnO_3$, the space group of bulk $BiMnO_3$ was determined to be $C2$ by one research group.[6,20] Actually, the same sample of $BiMnO_3$ (and the same structural model)[25] was used for the measurements of neutron powder diffraction data reported in two papers.[4,6] Their conclusion about space group $C2$ was based on their previous publication[20] where they observed the strong $h0l$ ($l=2n+1$) reflections [In Fig. 2(c) of Ref. 20, the indexes are given for the pseudocubic setting] by SAED. However, the $h0l$ ($l=2n+1$) reflections with this zone axis (probably [130] in the monoclinic setting) can appear due to the double diffraction in the case of $C2/c$ as well (see the simulated [130] SAED pattern for $C2/c$ in Table I). Therefore, one should find the correct [010] zone axis to determine whether the $h0l$ ($l=2n+1$) reflections are really present or not. In other words, the other axes that can be influenced by double diffraction cannot support the space

TABLE I. Simulated SAED patterns with the incident directions of [010], [−1−10], [0−1−1], [100], and [130], respectively, in terms of the space groups of $C2$ and $C2/c$. Simulations of the SAED patterns were based on dynamical diffraction theory.

	[010]	[0$\bar{1}\bar{1}$]	[$\bar{1}\bar{1}$0]	[100]	[130]
C2					
C2/c					

group determination. We should emphasize that all subsequent works accepted space group $C2$ without any doubt.

Here, we show the importance of discriminating the crystal axes of BiMnO$_3$ for the structural study in terms of SAED. The monoclinic structure of BiMnO$_3$ can be achieved by slightly distorting and rotating the MnO$_6$ octahedra in a simple cubic perovskite structure. Figure 1 is a schematic diagram that gives the relationship between the simple cubic perovskite lattice and monoclinic lattice of BiMnO$_3$.[6] The corners of the monoclinic unit cell are just located at the centers of the shaded cubic unit cells, as shown in Fig. 1. As seen in Fig. 1, the cubic structure has six equal directions, such as $[110]_p$, $[1-10]_p$, $[011]_p$, $[0-11]_p$, $[101]_p$, and $[-101]_p$, that can also be represented by $\langle 110 \rangle_p$ (p: pseudocubic). The distortion of the cubic lattice resulting in the monoclinic one, however, does not make a large difference on the SAED patterns from those of the cubic one. Therefore, monoclinic BiMnO$_3$ has also six corresponding incident directions that can give similar SAED patterns to each other.
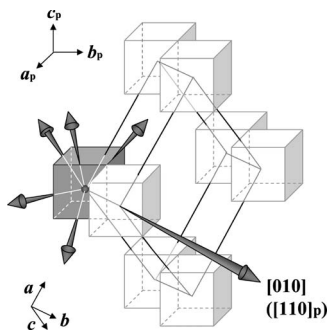
FIG. 1. Schematic diagram of relationship between the directions of the monoclinic and cubic lattices of BiMnO$_3$.

The first line of Table I shows the simulated SAED patterns at several incident directions of BiMnO$_3$ with the space group $C2$.[6] We should note that the arrangement of diffraction spots, for example, at the [010] incidence in terms of $C2$ ($C2$-[010]), is almost the same as that at $C2$-[−1−10]. Because of the feature of the SAED patterns taken from BiMnO$_3$, one should be careful in indexing SAED patterns, that is, in determining the incident directions for finding the extinction rules. However, measurement of lengths and angles between the electron diffraction spots is not very reliable that the slight differences between the SAED patterns seen in Table I can be distinguished. This is because the SAED patterns taken by any TEM are usually more or less deformed by the lenses through which the scattered electron beams pass depending on the conditions of the lenses, that is, TEM used for the study. From the facts, it is definitely worth to try to reinvestigate the space group of BiMnO$_3$.

In convergent-beam electron diffraction (CBED),[26,27] the diffraction pattern is obtained by using a conical electron beam on a specimen area less than 10 nm in diameter free from defects and grain and domain boundaries. Instead of the usual diffraction spots, diffraction disks are produced. Symmetry that can be seen in the CBED pattern including the higher-order Laue zone (HOLZ) reflections yield information on three-dimensional symmetry elements of the crystal structure around the zone axis parallel to the incident beam direction. Therefore, using CBED, the point group can be determined unambiguously, and then the incident directions of the SAED patterns can also be determined simultaneously. Most recently, the space group of BiMnO$_3$ was reported to be centrosymmetric $C2/c$ in terms of neutron powder diffraction, SAED, CBED,[18,22] and first-principles calculations.[21] These publications indicate that the space group of BiMnO$_3$ is not the established fact, and additional experiments are needed.

In our work, we have provided such additional experiments. We firstly observed the very weak but sharp $h0l$ ($l=2n+1$) and broader $h0l$ ($h=2n+1$) reflections by discriminating the crystal axes of BiMnO₃ using CBED and SAED at RT, which indicate the noncentrosymmetric long-range (space group $C2$) and short-range (space group $P2_1$ or $P2$) ordered structures, respectively. We also investigated the effects of heating and substitution of Sc and Cr for Mn on the very weak $h0l$ ($h=2n+1$ and $l=2n+1$) reflections.

II. EXPERIMENT

A mixture of Bi₂O₃ (99.99%) and Mn₂O₃ with an amount-of-substance ratio of 1:1 was placed in Au capsules and treated at 6 GPa in a belt-type high pressure apparatus at 1383 K for 60–70 min. After heat treatment, the samples were quenched to RT, and the pressure was slowly released. The resultant samples were black powder. X-ray powder diffraction (XRD) showed that the samples were single-phased. Single-phased Mn₂O₃ was prepared by heating commercial MnO₂ (99.99%) in air at 923 K for 24 h. Single-phased BiScO₃ was prepared from Bi₂O₃ and Sc₂O₃ (99.9%) at 6 GPa and 1413 K for 40 min,[24] and single-phased BiCrO₃ was prepared from Bi₂O₃ and Cr₂O₃ (99.9%) at 6 GPa and 1653 K for 120 min in Au capsules.[28] The solid solutions of BiMn₁₋ₓScₓO₃ were prepared from stoichiometric mixtures of Bi₂O₃, Sc₂O₃, and Mn₂O₃ in Au capsules at 6 GPa and 1443 K for 60–70 min.[29] XRD showed that BiMn₁₋ₓScₓO₃ contained a small amount of Bi₂O₂CO₃ as an impurity. By electron probe microanalysis (EPMA), in BiMnO₃, Bi:Mn =1.00(4):1.01–1.03(4) and in BiMn₀.₆Sc₀.₄O₃, Mn/Sc =1.58(16) and Bi/(Mn+Sc)=0.94(8) [the theoretical values are Mn/Sc=1.5 and Bi/(Mn+Sc)=1]. Therefore, within experimental errors, the composition is very close to the nominal composition. The bulk specimens were crushed and dispersed on carbon thin films on Cu grids for transmission electron microscopy. SAED and CBED patterns were taken at RT using an analytical TEM (Hitachi: HF-3000S) with a cold field emission gun operated at an accelerating voltage of 300 kV. High-temperature observation by SAED was performed at 673 K by using a heating holder (Gatan). The SAED and CBED patterns were taken from specimen areas of about 300 and 8 nm in diameters, respectively, using imaging plates. All SAED and CBED patterns were carefully taken with enough weak electron beams to avoid appearance of polymorph phases.[14–16] Simulations of the SAED patterns based on dynamical diffraction theory were carried out using the software MacTempas (Total Resolution LLC).

III. RESULTS AND DISCUSSIONS

A. Preliminary selected-area electron diffraction results

It was reported by off-resonant x-ray scattering experiment that in thin film BiMnO₃ sample, the $00l$ ($l=2n+1$) reflections can be observed, which indicates the absence of the c-glide plane.[9] The x-ray charge scattering ratios between $00l$ ($l=2n+1$) and 004 were, however, about 10^{-5}.[9] This is obviously beyond the detection limit of x-ray and neutron powder diffraction methods. Therefore, we decided to per-
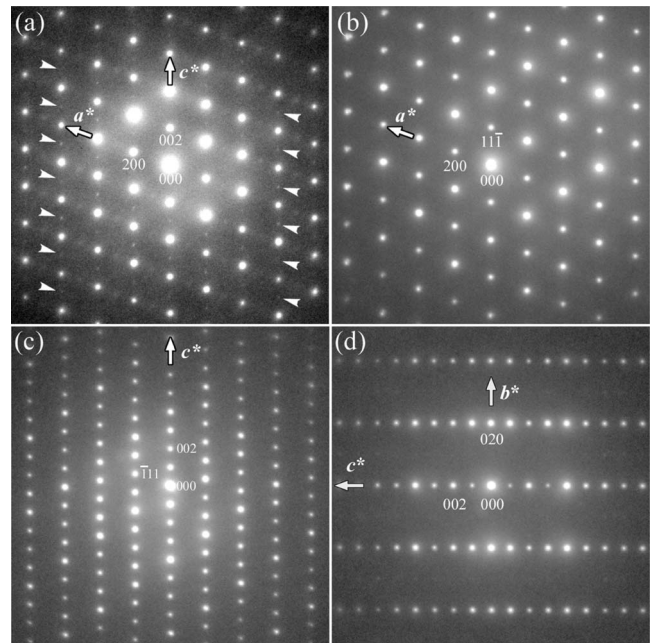
FIG. 2. SAED patterns taken from BiMnO₃ at RT with (a) [010], (b) [0−1−1] (c) [−1−10], and (d) [100] incident directions. The incident directions have been determined by CBED (Fig. 3).

form more careful SAED observations for BiMnO₃ compared with our previous works.[18,29] Figure 2 gives SAED patterns taken from BiMnO₃ with several zone axes. From Table I, Fig. 2(a) is possibly one of $C2$-[010], $C2$-[−1−10], or $C2/c$-[−1−10]. Similarly, the incident direction of Fig. 2(b) can also be one of $C2$-[0−1−1], $C2/c$-[010], or $C2/c$-[0−1−1]. Figure 2(c) can be one of $C2$-[010], $C2$-[−1−10], or $C2/c$-[−1−10]. Figure 2(d) can be $C2$-[100], $C2$-[130], $C2/c$-[100], or $C2/c$-[130]. Although the SAED patterns with $C2/c$-[130] and/or $C2$-[130] are slightly distorted in comparison with $C2/c$-[100] and/or $C2$-[100] ones, it is still difficult to discriminate those because of similarity of reflection arrangement. The forbidden $00l$ ($l=2n+1$) reflections of the $C2/c$-[100] and $C2/c$-[−1−10] SAED patterns can appear in the experimental SAED pattern due to double diffraction. For this reason, we performed CBED experiments as in the following section to distinguish the incident directions.

B. Convergent-beam electron diffraction results

Figure 3(a) is a CBED pattern taken from the same particle as that of Fig. 2(a). The ring-shaped reflections indicated by arrowheads occur from first-order Laue zone (FOLZ). Note here that if twofold rotational symmetry is observed in a CBED pattern, the incident direction must be uniquely determined to be a b axis ([010]) of the monoclinic lattice. The FOLZ reflections clearly show twofold rotational symmetry around the center of the CBED pattern where some of the FOLZ reflections are shown as a broader view. Therefore, the incident direction of Fig. 2(a) has been determined to be [010] incidence, that is, $C2$-[010].
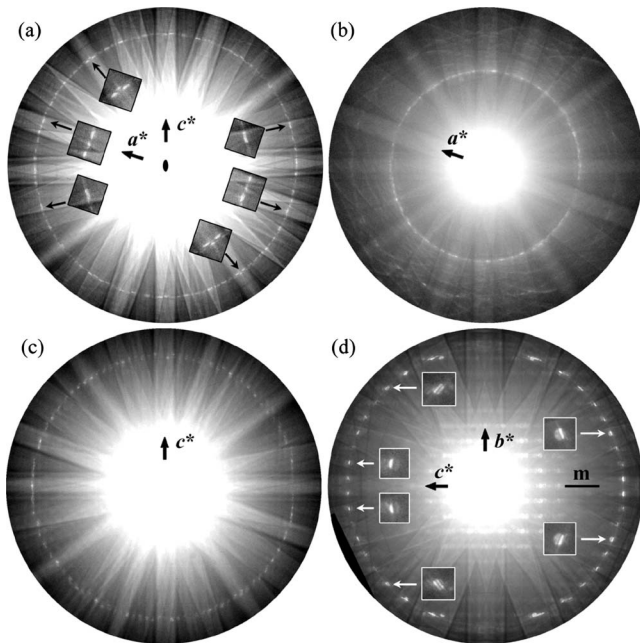
FIG. 3. CBED patterns taken from BiMnO$_3$ at RT with (a) [010] (b) [0$-$1$-$1] (c) [$-$1$-$10], and (d) [100] incident directions.

Figure 3(b) is the CBED pattern taken with the same direction as that of Fig. 2(b). Note that there are two different features between Figs. 3(a) and 3(b). First, the scattering angle of the HOLZ reflections of Fig. 3(b) is lower than that of Fig. 3(a). Second, Fig. 3(b) does not show twofold rotational symmetry. Figures 4(a) and 4(b) are schematic diagrams of FOLZ that can be seen in the CBED patterns with [010] and [0$-$1$-$1] incident directions, respectively. Note that the reciprocal lattice planes of Figs. 4(a) and 4(b) can be achieved by both the space groups of $C2/c$ and $C2$. From the
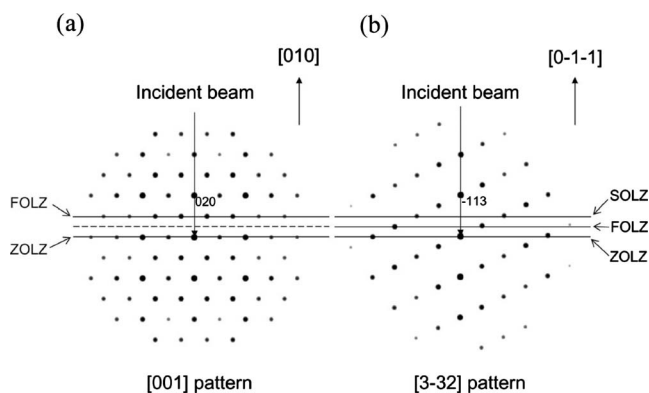
FIG. 4. Schematic diagrams of the HOLZ that can be seen in the CBED patterns with (a) [010] and (a) [0$-$1$-$1] incident directions, respectively. From the reciprocal lattice views with [001] and [3$-$32] that are perpendicular to [010] and [0$-$1$-$1] in (a) and (b), respectively, the first-order Laue zone (FOLZ) observed in the [0$-$1$-$1] CBED pattern must appear at half the scattering angle of the FOLZ observed in the [010] one. Note that the reciprocal lattices can be achieved by both space groups of $C2/c$ and $C2$. Here, SOLZ stands for the second-order Laue zone.

reciprocal lattice views with [001] and [3$-$32] that are perpendicular to [010] and [0$-$1$-$1], respectively, FOLZ observed in the [0$-$1$-$1] CBED pattern must appear at half the scattering angle of FOLZ observed in the [010] one. From this fact, candidates of the incident direction of Fig. 2(b) have been limited to be one of $C2$-[0$-$1$-$1] and $C2/c$-[0$-$1$-$1]. Figure 3(c) is the CBED pattern taken with the same direction as that of Fig. 2(c). The CBED pattern does not show twofold rotational symmetry. Thus, candidates of incident direction of Fig. 3(c) have been limited to be $C2$-[$-$1$-$10] and $C2/c-$[$-$1$-$10], indicating that Fig. 2(c) cannot be of $C2$-[010]. The results are summarized as follows; the incident directions of Figs. 2(a)–2(c) are $C2$-[010], $C2$-[0$-$1$-$1], and $C2$-[$-$1$-$10], respectively. Indexing of the SAED patterns has been performed as shown in Figs. 2(a)–2(c).

Note here that the weak but sharp $h0l$ ($l=2n+1$) reflections indicated by white arrowheads are found in this study with longer exposure time than in the previous work.[18] The SAED patterns in this study and in Ref. 18 were taken with the exposure times of 30 and 8 s, respectively. The $h0l$ ($l=2n+1$) reflections indicate the absence of the c-glide plane perpendicular to the b axis. The weak and broader $h0l$ ($h=2n+1$) reflections in Fig. 2(a) can be also observed, indicating the primitive monoclinic lattice with short-range order. We neglect the broader ones here and will discuss these in the next section.

Figure 3(d) is the CBED pattern taken with the same direction as that in Fig. 2(d). The CBED pattern clearly shows mirror symmetry perpendicular to the b axis. This indicates that Fig. 2(d) can be none of $C2$-[100], $C2$-[130], and $C2/c$-[130]. Then, the incident direction of Fig. 2(d) has uniquely been distinguished from the others and determined to be $C2/c$-[100]. This result, however, contradicts the SAED result of Fig. 2(a), indicating the absence of the c-glide plane. This implies that the $h0l$ ($l=2n+1$) reflections are too weak to influence the [100] HOLZ CBED pattern, resulting in mirror symmetry.[30] The $h0l$ ($l=2n+1$) reflections that should be absent due to a c-glide plane perpendicular to the b axis appear in Fig. 2(d). The reflections, however, can appear in the [100] SAED pattern by the dynamical electron diffraction effect (double diffraction effect). Figure 5 is a [100] CBED pattern including only zero-order Laue zone (ZOLZ) reflections. The dynamical extinction lines (GM line)[26,27] are clearly seen in the $00l$ ($l=2n+1$) reflection disks of the CBED pattern, indicating the existence of the c-glide plane perpendicular to the b axis. The inconsistency between the [100] ZOLZ CBED pattern and the [010] SAED pattern is also due to negligible influence of the $00l$ ($l=2n+1$) reflections.[30] From the results, the space group of BiMnO$_3$ can be determined to be centrosymmetric $C2/c$ in terms of CBED, as we reported previously,[18] although the space group can be $C2$ if we take into consideration the $h0l$ ($l=2n+1$) reflections seen in the [010] SAED pattern. In the next section, the $h0l$ ($l=2n+1$) reflections as well as the $h0l$ ($h=2n+1$) ones will be discussed in detail.
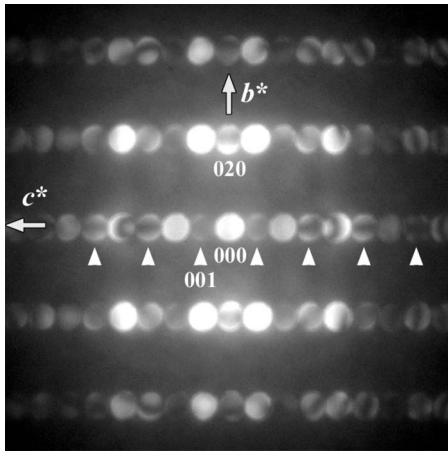
FIG. 5. [100] CBED pattern including only ZOLZ reflection disks at RT. The dynamical extinction lines (GM lines) along the c^* direction, indicating the c-glide plane perpendicular to the b axis, can be clearly seen at $00l$ ($l=2n+1$).

C. Long-range and short-range structural orders in BiMnO₃ figured out by detailed selected-area electron diffraction analysis

Figure 6(a) is the [010] SAED pattern taken from BiMnO₃ at RT. As indicated by the arrowheads in Fig. 6(a), the broader $h0l$ ($h=2n+1$) reflections indicating short-range structural order are observed as well as the $h0l$ ($l=2n+1$) reflections indicating long-range structural order ($C2$) of BiMnO₃. If both reflections are also taken into consideration, the space group should be $P2$ or $P2_1$. In any case, there is no
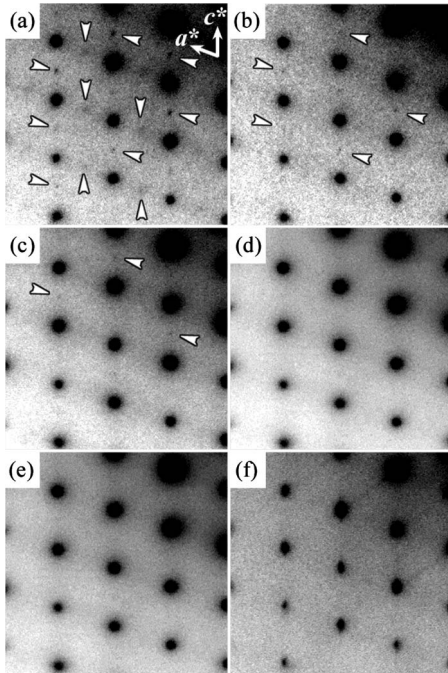
FIG. 6. [010] SAED patterns taken from BiMn₁₋ₓScₓO₃ at room temperature with (a) $x=0$, (b) $x=0.1$, (c) $x=0.4$, (d) $x=0.7$, and (e) $x=1.0$ and from (f) BiCrO₃.
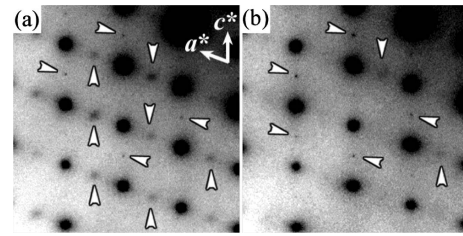
FIG. 7. [010] SAED patterns taken from BiMnO₃ at (a) RT and (b) 673 K.

mirror symmetry in terms of point symmetry.

Figures 6(b)–6(e) are [010] SAED patterns taken at RT from the BiMn₁₋ₓScₓO₃ samples with $x=0.1$, 0.4, 0.7, and 1.0, respectively. For $x=0.1$, the $h0l$ ($h=2n+1$) reflections disappear while the $h0l$ ($l=2n+1$) reflections still survive [Fig. 6(b)]. On the other hand, it can be seen that the intensities of the $h0l$ ($l=2n+1$) reflections decrease with substitution of Sc for Mn. The reflections persist up to $x=0.4$ [Fig. 6(c)] and almost disappear at $x=0.7$ [Fig. 6(d)]. The result for $x=1.0$ [Fig. 6(e)] where the $h0l$ ($l=2n+1$) reflections are not seen at all is consistent with another recent work.[24] Figure 6(f) is a SAED pattern taken from the isostructural BiCrO₃ (Ref. 28) sample with the [010] incidence. The $h0l$ ($h=2n+1$ and $l=2n+1$) reflections are also absent, indicating that BiCrO₃ has a C-centered cell and a c-glide plane, and therefore has space group $C2/c$. Quite recently, BiCrO₃ was shown to have antiferroelectric properties.[31] This result confirms that BiCrO₃ crystallizes in a centrosymmetric crystal structure. The results on BiScO₃ and BiCrO₃ obtained in this work indicate that the long-range ordered noncentrosymmetric structure of BiMnO₃ at RT is attributed not only to Bi³⁺ ions with lone electron pair but also to Mn³⁺ ions, that is, to correlation between Bi³⁺ ions and Mn³⁺ ions. The intensities of the observed $h0l$ ($l=2n+1$) reflections are much weaker than the intensities of these reflections in the previous works.[10,14,16,20]

Figures 7(a) and 7(b) are [010] SAED patterns taken from BiMnO₃ at RT and 673 K, respectively. Similar to Fig. 6(b) of BiMn₀.₉Sc₀.₁O₃, most of the $h0l$ ($h=2n+1$) reflections seen in Fig. 7(a) disappear in Fig. 7(b) although the $h0l$ ($l=2n+1$) reflections still survive, as indicated by the arrowheads. The disappearance of the $h0l$ ($h=2n+1$) reflections at 673 K shows that the only short-range ordered structure with the lattice type P disappeared. Our high-temperature observation does not contradict with the results of the resonant x-ray study where the off-resonant peak persisted up to 600 K, as seen in Fig. 4 of Ref. 9. Heating the BiMnO₃ sample to 673 K and substitution of 10% Sc for Mn result in the same effect on the $h0l$ ($h=2n+1$) reflections. Note that the disappearance of $h0l$ ($h=2n+1$) reflections in BiMnO₃ on heating confirms that these reflections are intrinsic and not caused, for example, by electron beam irradiation effect. It has also been confirmed from SAED that the monoclinic angle β in BiMnO₃ decreases by about 2° at high temperature and in BiMn₀.₉Sc₀.₁O₃ at RT in comparison with β of BiMnO₃ at RT. These results are consistent with the recent results obtained by neutron powder diffraction analysis

where this type of distortion is attributed to the disappearance of cooperative static Jahn-Teller distortions.[18,29] We could not achieve the *Pbnm* orthorhombic phase[5] by heating the $BiMnO_3$ sample because the structure was changed to one of the polymorph phases[14–16] around 773 K, and the sample was destroyed soon after that.

It can be considered from the findings in this study that the $h0l$ ($h=2n+1$) reflections in $BiMnO_3$ are related to the orbital order, while the $h0l$ ($l=2n+1$) reflections are not likely related to the orbital order because the reflections persist up to high temperature above the monoclinic-to-monoclinic phase transition where the cooperative static Jahn-Teller distortion is believed to be suppressed.[18,29] On the other hand, the $h0l$ ($h=2n+1$) reflections drastically disappear at high temperature. This fact shows that the monoclinic-to-monoclinic phase transition is accompanied by the change in the crystal symmetry, in contrast to the general belief that there is no symmetry change.[5,10–12]

We should note that the weak reflections might be possibly originated from other crystal domains whose incident direction is $[-1-10]$ [Fig. 2(c)]. However, no features (no mismatching between them in the SAED pattern or no splitting diffraction spots) due to such domain structures could be seen in the [010] SAED pattern and the dark-field TEM image taken by using one of the weak reflections so far.

The observation of the weak $h0l$ ($h=2n+1$ and $l=2n+1$) reflections by SAED shows that good single crystals of $BiMnO_3$ are obviously needed for careful structure analysis and understanding of the origin of the ordered structures found in this study. X-ray and neutron powder diffraction data cannot give unambiguous information about the origin of the ordered structures because of the following reasons.

(1) For the (001), (002), and (004) reflections, the intensity ratios calculated from the structure parameters refined in the $C2$ model are 0.07 (Atou *et al.*),[6] 0.03 (Moreira dos Santos *et al.*),[4] and 0.008 (Belik *et al.*)[18] for $I(001)/I(004)$ and 0.02 (Atou *et al.*),[6] 0.02 (Moreira dos Santos *et al.*),[4] and 0.004 (Belik *et al.*)[18] for $I(002)/I(004)$ for XRD data with Cu $K\alpha$ radiation. That is, the calculated $I(001)/I(004)$ ratio is larger than the $I(002)/I(004)$ one. The (002) reflection can be detected by XRD. We also found that separate peaks with the intensity ratio of 0.002 compared with the (004) reflection can still be detected by XRD. However, no $h0l$ ($h=2n+1$ and $l=2n+1$) reflections were observed experimentally even when XRD data were collected with very long exposure time (480 s/step; a RIGAKU Ultima III diffractometer with Cu $K\alpha$ radiation). In addition, the calculated intensity ratios $I(001)/I(004)$ and $I(003)/I(004)$ are much larger than the experimentally measured ones of about 10^{-5} for thin film samples.[9]

(2) The structural model including the short-range ordered one at RT should have space groups $P2$ or $P2_1$, and the number of refined structural parameters is about four times larger than that of the $C2/c$ model. However, difficulties in the structure refinement already appear in the $C2$ model where the number of refined structural parameters is about two times larger than that of the $C2/c$ model.[18] These difficulties include strong dependence of structural and thermal parameters (and therefore bond lengths) on tiny changes of

nonstructural parameters reflecting probably a number of local minima.[18] It can explain quite different calculated polarizations (18.96 and 0.9 $\mu C/cm^2$)[21] for the reported crystal structures[4,6] even when the same sample was used in these works.[25]

The space group determined in terms of CBED ($C2/c$) is in agreement with the results of first-principles calculations.[21] As emphasized in Ref. 21, the calculations were performed for ideal stoichiometric $BiMnO_3$. Stoichiometry may be the key word for understanding the structural properties of $BiMnO_3$. Our $BiMnO_3$ sample had no impurities, and EPMA gave the stoichiometric composition within the experimental errors. Nevertheless, tiny changes or fluctuations in stoichiometry are always possible especially on nanoscale. By introduction of structural defects, the ideal centrosymmetric structure may relax to a structure with lower symmetry. Because it was shown that the ideal $C2/c$ structure is more stable than the $C2$ structure, additional symmetry reduction takes place by removing the C-centered monoclinic cell. The probability of compositional fluctuation within the sample region of about 300 nm in diameter (the selected region for SAED) is much larger than that of about 8 nm in diameter (the probe size of electron beam on the sample for CBED). Sc has the robust oxidation state +3 compared with Mn where Mn^{2+}, Mn^{3+}, and Mn^{4+} oxidation states are possible (for example, the presence of Mn^{2+} and Mn^{4+} may locally change the oxygen content, keeping the Bi:Mn ratio as 1:1). Therefore, the introduction of Sc^{3+} ions may significantly reduce compositional fluctuation, and we observe noticeable reduction of the intensities of the $h0l$ ($l=2n+1$) reflections with increasing the Sc content (Fig. 6), that is, approaching the ideal structure. Cr^{3+} is also a very stable oxidation state. Therefore as a result, $BiScO_3$ and $BiCrO_3$ adopt the ideal $C2/c$ structure [Figs. 6(e) and 6(f)]. More complicated superstructures in $BiMnO_3$ are formed due to the creation of oxygen defects under electron beam irradiation.[14–16] This fact shows that stoichiometry has a strong effect on the structural properties of $BiMnO_3$. The cation nonstoichiometry (for example, due to the presence of $Bi_2O_2CO_3$ in some samples) in $BiMnO_3$ may also significantly enhance deviation from the ideal structure and give rise to strong $h0l$ ($l=2n+1$) reflections.

To the best of our knowledge, ferroelectric properties of monoclinic $BiScO_3$ have not been investigated yet. One paper reported that $BiScO_3$ thin films (having, however, a tetragonal structure) did not exhibit ferroelectric or antiferroelectric properties.[32] However, monoclinic $BiScO_3$ should be antiferroelectric by analogy with monoclinic $BiCrO_3$.[31] Thin film samples of $BiMnO_3$ have a polar structure shown by second-harmonic generation.[23] As we mentioned in Sec. I, the ferroelectric properties of $BiMnO_3$ (ferroelectric hysteresis loop) were shown only in one work[8] and have not been confirmed by other groups despite of many efforts. There are a growing number of publications emphasizing that ferroelectric properties of $BiMnO_3$ have not been well established.[33] The symmetry of bulk $BiMnO_3$ determined in this work allows it to be ferroelectric. Therefore, in $BiMnO_3$-$BiScO_3$ solid solutions, one may expect gradual change of properties from ferroelectric (if any) to antiferroelectric. The conductivity of $BiMn_{1-x}Sc_xO_3$ thin films may

be considerably reduced compared with that of BiMnO$_3$, making the investigation of ferroelectric properties of BiMn$_{1-x}$Sc$_x$O$_3$ possible.

IV. CONCLUSION

We investigated the space group of BiMnO$_3$ by using CBED and SAED. CBED used for discrimination for the crystal axes of BiMnO$_3$ showed that BiMnO$_3$ belongs to point group $2/m$ with the c-glide plane perpendicular to the b axis, resulting in space group $C2/c$. In the SAED patterns, however, the very weak but sharp $h0l$ $(l=2n+1)$ and broader $h0l$ $(h=2n+1)$ reflections were observed, indicating the noncentrosymmetric long-range (space group $C2$) and short-range ordered structures ($P2$ or $P2_1$), respectively, implying that such weak reflections had quite little influence on the CBED patterns. At the same time, it was figured out that CBED is crucial in order to discriminate the crystal axes of

BiMnO$_3$ for the structural study based on the comparatively strong reflections. We also investigated the effects of substitution of Sc and Cr for Mn and of heating on the very weak $h0l$ ($h=2n+1$ and $l=2n+1$) reflections, respectively. It was revealed based on substitution effect that the noncentrosymmetric long-range ordered structure ($C2$) of BiMnO$_3$ is attributed not only to Bi^{3+} ions with lone electron pair but also to Mn^{3+} ions, that is, to correlation between Bi^{3+} ions and Mn^{3+} ions. The results of this work are important for understanding multiferroic properties of BiMnO$_3$.

*Corresponding author; yokosawa.tadahiro@nims.go.jp

[1] For recent reviews, see W. Eerenstein, N. D. Mathur, and J. F. Scott, Nature (London) **442**, 759 (2006); D. I. Khomskii, J. Magn. Magn. Mater. **306**, 1 (2006); M. Fiebig, J. Phys. D **38**, R123 (2005); N. A. Hill, Annu. Rev. Mater. Res. **32**, 1 (2002); S. W. Cheong and M. Mostovoy, Nat. Mater. **6**, 13 (2007); R. Ramesh and N. A. Spaldin, Nat. Mater. **6**, 21 (2007).

[2] N. A. Hill, J. Phys. Chem. B **104**, 6694 (2000).

[3] F. Sugawara, S. Iiida, Y. Syono, and S. Akimoto, J. Phys. Soc. Jpn. **25**, 1553 (1968).

[4] A. Moreira dos Santos, A. K. Cheetham, T. Atou, Y. Syono, Y. Yamaguchi, K. Ohoyama, H. Chiba, and C. N. R. Rao, Phys. Rev. B **66**, 064425 (2002).

[5] T. Kimura, S. Kawamoto, I. Yamada, M. Azuma, M. Takano, and Y. Tokura, Phys. Rev. B **67**, 180401(R) (2003).

[6] T. Atou, H. Chiba, K. Ohoyama, Y. Yamaguchi, and Y. Syono, J. Solid State Chem. **145**, 639 (1999).

[7] R. Seshadri and N. A. Hill, Chem. Mater. **13**, 2892 (2001); N. A. Hill and K. M. Rabe, Phys. Rev. B **59**, 8759 (1999).

[8] A. Moreira dos Santos, S. Parashar, A. R. Raju, Y. S. Zhao, A. K. Cheetham, and C. N. R. Rao, Solid State Commun. **122**, 49 (2002).

[9] C. H. Yang, J. Koo, C. Song, T. Y. Koo, K. B. Lee, and Y. H. Jeong, Phys. Rev. B **73**, 224112 (2006).

[10] E. Montanari, L. Righi, G. Calestani, A. Migliori, E. Gilioli, and F. Bolzoni, Chem. Mater. **17**, 1765 (2005).

[11] E. Montanari, G. Calestani, A. Migliori, M. Dapiaggi, F. Bolzoni, R. Cabassi, and E. Gilioli, Chem. Mater. **17**, 6457 (2005).

[12] Z. H. Chi, C. J. Xiao, S. M. Feng, F. Y. Li, C. Q. Jin, X. H. Wang, R. Z. Chen, and L. T. Li, J. Appl. Phys. **98**, 103519 (2005).

[13] W. Eerenstein, F. D. Morrison, J. F. Scott, and N. D. Mathur, Appl. Phys. Lett. **87**, 101906 (2005).

[14] Z. Chi, H. Yang, F. Li, R. Yu, C. Jin, X. Wang, X. Deng, and L. Li, J. Phys.: Condens. Matter **18**, 4371 (2006).

[15] H. Yang, Z. H. Chi, F. Y. Li, C. Q. Jin, and R. C. Yu, Phys. Rev. B **73**, 024114 (2006).

[16] H. Yang, Z. H. Chi, L. D. Yao, W. Zhang, F. Y. Li, C. Q. Jin, and R. C. Yu, J. Appl. Phys. **100**, 044105 (2006).

[17] T. Shishidou, N. Mikamo, Y. Uratani, F. Ishii, and T. Oguchi, J.

Phys.: Condens. Matter **16**, S5677 (2004).

[18] A. A. Belik, S. Iikubo, T. Yokosawa, K. Kodama, N. Igawa, S. Shamoto, M. Azuma, M. Takano, K. Kimoto, Y. Matsui, and E. Takayama-Muromachi, J. Am. Chem. Soc. **129**, 971 (2007).

[19] A. A. Belik and E. Takayama-Muromachi, Inorg. Chem. **45**, 10224 (2006).

[20] H. Chiba, T. Atou, H. Faqir, M. Kikuchi, Y. Syono, Y. Murakami, and D. Shindo, Solid State Ionics **108**, 193 (1998).

[21] P. Baettig, R. Seshadri, and N. A. Spaldin, J. Am. Chem. Soc. **129**, 9854 (2007).

[22] E. Montanari, G. Calestani, L. Righi, E. Gilioli, F. Bolzoni, K. S. Knight, and P. G. Radaelli, Phys. Rev. B **75**, 220101(R) (2007).

[23] A. Sharan, J. Lettieri, Y. Jia, W. Tian, X. Pan, D. G. Schlom, and V. Gopalan, Phys. Rev. B **69**, 214109 (2004).

[24] A. A. Belik, S. Iikubo, K. Kodama, N. Igawa, S. Shamoto, M. Maie, T. Nagai, Y. Matsui, S. Yu. Stefanovich, B. I. Lazoryak, and E. Takayama-Muromachi, J. Am. Chem. Soc. **128**, 706 (2006).

[25] A. K. Cheetham (private communication).

[26] M. Tanaka, Acta Crystallogr., Sect. A: Found. Crystallogr. **50**, 261 (1994).

[27] D. B. Williams and C. B. Carter, *Transmission Electron Microscopy—A Textbook for Materials Science* (Plenum, New York, 1996).

[28] A. A. Belik, N. Tsujii, H. Suzuki, and E. Takayama-Muromachi, Inorg. Chem. **46**, 8746 (2007).

[29] A. A. Belik, T. Yokosawa, K. Kimoto, Y. Matsui, E. Takayama-Muromachi, Chem. Mater. **19**, 1679 (2007).

[30] M. Tanaka, M. Terauchi, and T. Kaneyama, *Convergent-Beam Electron Diffraction II* (JEOL, Tokyo, 1988), pp. 120–139.

[31] D. H. Kim, H. N. Lee, M. Varela, and H. M. Christen, Appl. Phys. Lett. **89**, 162904 (2006).

[32] M. Murakami, M. A. Aronova, M. Wuttig, I. Takeuchi, S. Trolier-McKinstry, K. McDonald, E. Knoesel, S. E. Lofland, T. Chikyow, T. Aoyama, and K. Nakajima, Philos. Mag. Lett. **87**, 241 (2007).

[33] W. Eerenstein, F. D. Morrison, F. Sher, J. L. Prieto, J. P. Attfield, J. F. Scott, and N. D. Mathur, Philos. Mag. Lett. **87**, 249 (2007).